Am J Cancer Res 2022;12(8):3947-3966
www.ajcr.us /ISSN:2156-6976/ajcr0144023

Original Article

The potential value of cuprotosis (copper-induced cell death) in the therapy of clear cell renal cell carcinoma

Xiaochen Qi, Jin Wang, Xiangyu Che, Quanlin Li, Xiaowei Li, Qifei Wang, Guangzhen Wu

Department of Urology, The First Affiliated Hospital of Dalian Medical University, Dalian 116011, Liaoning, China

Received May 9, 2022; Accepted July 20, 2022; Epub August 15, 2022; Published August 30, 2022

Abstract: Clear cell renal cell carcinoma (ccRCC) accounts for 75% of the total incidence of renal cancer, and every year the number of morbidity and mortality increases, posing a serious threat to public health. The current main treatment methods for kidney cancer include drug-targeted therapy and immunotherapy. Although there are many treatment options for kidney cancer, they all have limitations, including drug resistance, unsatisfied long-term benefits, and adverse effects. Therefore, it is crucial to identify more effective therapeutic targets. As a newly discovered mechanism of cell death, copper-induced cell death (cuprotosis) is closely related to changes in cell metabolism, particularly in copper metabolism. Current studies have shown that the key signaling pathway of cuprotosis, the FDX1 (Ferredoxin 1)-LIAS (Lipoic Acid Synthetase) axis, plays an important role in the regulation of cellular oxidative stress, which can directly affect cell survival via inducing or promoting cancer cell death. Therefore, we speculated that this regulatory cell death mechanism might serve as a potential therapeutic target for the clinical treatment of renal cancer. To test this, we first performed a pan-cancer analysis based on cuprotosis-related genomic and transcriptomic levels to reveal the expression of cuprotosis in cancer. Next, GSVA-clustering analysis was performed with data from the Cancer Genome Atlas (TCGA) cohort, and the cohort was divided into three clusters according to the gene enrichment levels of cuprotosis marker genes. In addition, we analyzed the potential of using cuprotosis in clinical treatment from multiple perspectives, including chemotherapeutic drug susceptibility test, immune target inhibition treatment responsiveness, and histone modification. Combining the results of multi-omics analysis, we focused on the feasibility of this novel regulatory cell death mechanism in ccRCC treatment and further constructed a prognostic model. Finally, we verified our results by integrating the patient's gene expression information and radiomics information. Our study provides new insights into the development and clinical application of targeting cuprotosis pathway.

Keywords: Cuprotosis, regulatory cell death, bioinformatics, radiomatics, immune checkpoint inhibitor, tumor mutation burden

Introduction

Copper is one of the essential components of all living organisms. Copper ions play a critical role in maintaining cell homeostasis. However, excessive copper concentration can lead to cell death [1], a new form of cell death named cuproptosis, discovered by Peter's team in March 2022 [2]. Although the mechanisms of toxicity of other metals, such as iron, have been well established, the mechanism by which copper induces cell death is poorly understood. Recent studies have found that cuproptosis, unlike other forms of cell death, occurs primarily through the direct binding of copper to the fatty acylated component of the Krebs cycle, which leads to the aggregation of fatty acylated proteins and the subsequent loss of iron-sulfur clusterin, thereby leading to increased protein toxicity and ultimately cell death [1, 2]. Nevertheless, comprehensive study, particularly, pan-cancer analysis of cuproptosis will help reveal the role of cuproptosis in tumor biology. In this study, we analyzed the expression of cuproptosis, identified 17 classic key genes involved in cuproptosis, and determined the expression, prognosis, gene variation and expression of cuproptosis in different tumors through pan-cancer analysis. We found that cuproptosis-related genes were markedly down-regulated in renal clear cell carcinoma, and the expression of these genes was posi-

https://doi.org/10.62347/ETJH6697

tively correlated with prognosis, suggesting the clinical implication of cuproptosis in renal cancer.

ccRCC is the predominant histological subtype of renal cell carcinoma, accounting for approximately 75% of renal cell carcinomas [3]. Despite considerable clinical efforts, the recurrence and the increasing incidence still make ccRCC a medical challenge [4]. Therefore, it is essential to identify new therapeutic targets to improve the diagnosis and prognosis of ccRCC [5]. Normal cells mainly metabolize glucose through the tricarboxylic acid cycle, while tumor cell proliferation utilizes glucose mainly through aerobic glycolysis, which is known as the Warburg effect. Glycolysis products undergo de novo synthesis of fatty acids to form a large quantity of fatty acids by the action of important fatty acid synthases, such as Fatty Acid Synthase (FASN), Stearoyl-CoA Desaturase 1 (SCD1), Sterol Regulatory Element Binding Transcription Factor 1c (SREBP-1c), and Acetyl-CoA Carboxylase (ACC). These fatty acids provide energy sources for the proliferation and metastasis of renal clear cell carcinoma and are also important raw materials to produce cell signaling molecules and the synthesis of cell membranes.

In addition, fatty acids also participate in the epithelial-mesenchymal transition (EMT) process of tumor cells by regulating the structure of tumor cell membranes, thereby regulating tumor invasion and metastasis [6-10]. The dependence of cuproptosis on the tricarboxylic acid cycle is contradictory to the reported fat metabolism in renal cancer. Therefore, understanding the specific regulatory mechanism of cuproptosis in renal cancer cells is important for the treatment of renal cancer. In this study, we first performed a various bioinformatics study to determine the association of cuproptosis with the immune features and the prognosis of renal cancer. We further constructed a new model of renal cancer prognosis. Finally, given the current problem of drug selection and resistance in patients undergoing targeted therapy and immunotherapy, we randomly selected the CT images of 75 TCGA samples from The Cancer Imaging Archive (TCIA) database [11] according to cuproptosis type and constructed 5 prediction models of different types of cuproptosis with the help of 5 different classifiers by checking the ROI (region of Interest) of lesion and extracting its image characteristics by using pyradiomics [12]. Findings from our study will help understand the role of copper-related death in renal clear cell carcinoma.

Material and method

Data collection

The clinicopathological information and gene expression matrix of ccRCC patients were obtained from the TCGA database and the ArrayExpress database. ccRCC cell line expression profiles and anticancer drug data were obtained from the Genomics of Drug Sensitivity in Cancer (GDSC database). The protein expression levels of ccRCC patients and the immunohistochemical and immunofluorescence results of ccRCC cells were obtained from the Clinical proteomic tumor analysis consortium (CPTAC) database. CT images of TCGA ccRCC cohort patients were obtained from the TCIA database [11].

Bioinformatics analysis

GSVA algorithm was used to calculate the cuprotosis enrichment score of a single sample to obtain the cuprotosis-score of each sample [18]. Cluster analysis according to the expression level of the samples was implemented using ward.D [19]. In our cluster analysis, we relied on cuprotosis-score for clustering, and cuprotosis-score was obtained by GSVA algorithm, i.e., each sample or single cell was sorted by gene expression, and then all samples were sorted by gene expression. The value of the enrichment score was normalized, and cuprotosis-score was the result obtained after normalizing the GSVA enrichment score of each sample, so it represented the expression level of each gene in each sample based on the cuprotosis gene set, which could objectively reflect the difference in the expression level of cuprotosis in each sample. Based on the pRRophetic algorithm [20], we constructed a ridge regression model to predict drug IC50 based on the TCGA database and the expression profile of GDSC cell lines. Using the TIDE algorithm (http://tide.dfci.harvard.edu/) and submap algorithm from GenePattern (https://cloud.genepattern.org/gp), we predicted the possibility of response to immunotherapy for three cuprotosis cluster subtypes. Immune-

related analysis scores were implemented using seven algorithms: CIBERSORT, CIBERSORT-ABS, ESTIMATE, MCPcounter, XCELL, EPIC and TIMER. ssGSEA algorithm was used to quantify the degree of immune cell infiltration based on TCGA data [21]. T test, univariate COX regression, and least absolute shrinkage and selection operator (LASSO) regression were used to screen genes and image features, and multivariate COX regression was used to construct prognostic models. Five machine learning algorithms including random forest, support vector machine, Xgboost, MLP and Lightgbm were used to construct a prediction model of cuprotosis expression based on image features.

* was used to represent *p* value of all statistical analysis results. *: P<0.05; **: P<0.01; ***: P<0.001; ****: P<0.0001.

Programming languages, software and major software packages (libraries)

R (4.1.1): Survival analysis and COX regression analysis: survival, limma, survminer.

Cluster analysis: consensuscluster, hclust.

LASSO regression analysis: glmnet.

Plotting: ggplot2, ggstatsplot, corrplot, vioplot, forestplot, rms.

Python (3.9): Obtain image omics features: pyradiomics.

Machine learning algorithm: sklearn.

3D slicer: delineate areas of interest (ROI).

Perl: CNV and SNV of cuprotosis-related genes in each cancer type were calculated by perl language.

Results

Pan-cancer analysis of cuprotosis

Although studies on the cancer-related aspects of cuprotosis are limited, there are emerging reports on the functional mechanism of cuprotosis and the key genes in cuprotosis pathway (**Figure 1A**) [1, 22-24]. Hence, we selected 17 cuprotosis-related genes from relevant literature for our current study: CDKN2A, GCSH, ATP7B, LIPT1, GLS, PDHA1, DLD, ATP7A, DLST, SLC31A1, LIAS, FDX1, DLAT, PDHB, MPC1, MTF1, DBT. By analyzing normal and cancer cohort samples in the TCGA database, we found that mutations and differential expressions of cuprotosis-related genes were widely present in a variety of cancers (**Figure 1B-E**). Mutations were particularly evident in some high-incidence cancers, such as UCEC, COAD, and PCPG. Among the 33 cancers examined, except for SKCM, THYM and PAAD, cuprotosis-related genes were significantly differentially expressed between cancer and normal tissues. In ccRCC, most of the cuprotosis-related genes were expressed at low level. In consistent with this, survival landscape analysis of the samples showed that the expression of most of the cuprotosis-related genes was correlated with the favorable prognosis of patients with ccRCC (**Figure 1G**, **1I**). These results were also validated by immunofluorescence staining of different cancer cell lines, such as A-431 and A-OS-2, in the CPTAC database (**Figure 1F**). We further expressed the influence weights of these genes in different oncogenic/tumor-suppressor pathways by fan graph (**Figure 1H**). The results showed that cuprotosis-related genes affected many signaling pathways, especially the RTK, EMT, and cell cycle pathways [25-29], which were important in cancer cell proliferation and metastasis, suggesting that cuprotosis-related genes are closely associated with the development of cancer.

Clustering analysis of TCGA ccRCC samples and anticancer drug sensitivity prediction

Currently, targeted therapy is the main treatment method for ccRCC [30]. Therefore, it is essential to determine whether there is a correlation between cuprotosis and various targeted drugs and to predict whether the differential expression of cuprotosis will affect the sensitivity of ccRCC to various anticancer drugs. Using the expression levels of cuprotosis-related genes in normal cohort samples as a reference, we conducted an unsupervised clustering analysis and divided TCGA ccRCC cohort samples into three clusters based on the expression levels (**Figure 2A**): Cluster1 (cuprotosis medium expression), Cluster2 (cuprotosis low expression), and Cluster3 (cuprotosis high expression) (**Figure 2B**). The violin plot showed that there were noticeable differences in gene enrichment among the three clusters, and the survival curve also

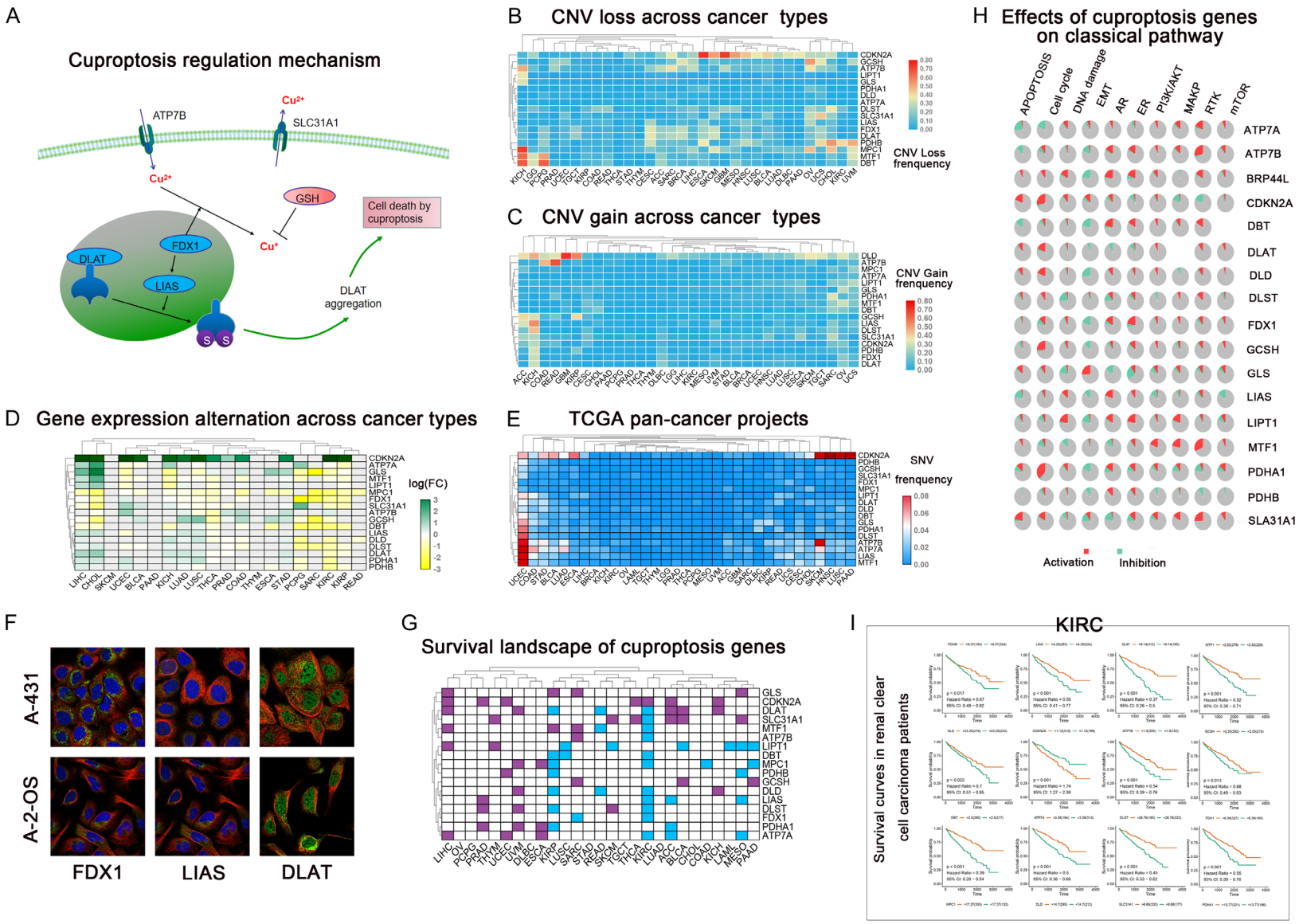
A
Cuproptosis regulation mechanism
ATP7B
SLC31A1
Cu2+
Cu2+
GSH
Cell death by cuproptosis
Cu+
FDX1
DLAT
LIAS
DLAT aggregation
B CNV loss across cancer types
CNV Loss frenquency
C CNV gain across cancer types
CNV Gain frenquency
D Gene expression alternation across cancer types
log(FC)
E TCGA pan-cancer projects
SNV frenquency
H Effects of cuproptosis genes on classical pathway
APOPTOSIS
Cell cycle
DNA damage
EMT
AR
ER
PI3K/AKT
MAPK
RTK
mTOR
ATP7A
ATP7B
BRP44L
CDKN2A
DBT
DLAT
DLD
DLST
FDX1
GCSH
GLS
LIAS
LIPT1
MTF1
PDHA1
PDHB
SLA31A1
Activation
Inhibition
F
A-431
A-2-OS
FDX1
LIAS
DLAT
G
Survival landscape of cuproptosis genes
I
KIRC
Survival curves in renal clear cell carcinoma patients

Figure 1. Pan-cancer analysis and molecular mechanism. A. The mechanism of cell death caused by cuprotosis. The massive accumulation of DLAT bound to sulfur atoms is the direct cause of cuprotosis. B, C. CNV (copy number variation) representation of Cuprotosis-related genes in 33 cancers. B, C. Represent CNV gain and CNV loss, respectively. The color bar on the right represents the CNV gain/loss frenquency, from blue to red corresponding to the degree from low to high. D. The heat map shows the expression of cuprotosis-related genes in 33 cancers after taking the logarithm of the ratio of expression levels in cancer and normal tissues. The color bar on the right indicates that the color from yellow to green corresponds to the ratio of expression levels from low to high. E. SNV (single nucleotide variation) representation of Cuprotosis-related genes in 33 cancers. The color bar on the right represents the SNV frenquency, from blue to red corresponding to the degree from low to high. F. Immunofluorescence showed the expression distribution of the proteins corresponding to the three key genes (FDX1, LIAS, DLAT) in curoptosis in A-2-OS and A-431 cell lines. G. Combined with the survival information of the samples, the properties of cuprotosis-related genes in 33 cancers were judged, and they were classified as protective genes or risk genes. Among them, blue represents protective genes and purple represents risk genes. H. The roles and weights of cuprotosis-related genes in various classical oncogenic pathways, blue represents activation and red represents inhibition. I. Survival curves of 12 curoptosis-related genes with statistical significance in ccRCC based on their expression levels and the clinical survival information of the samples.

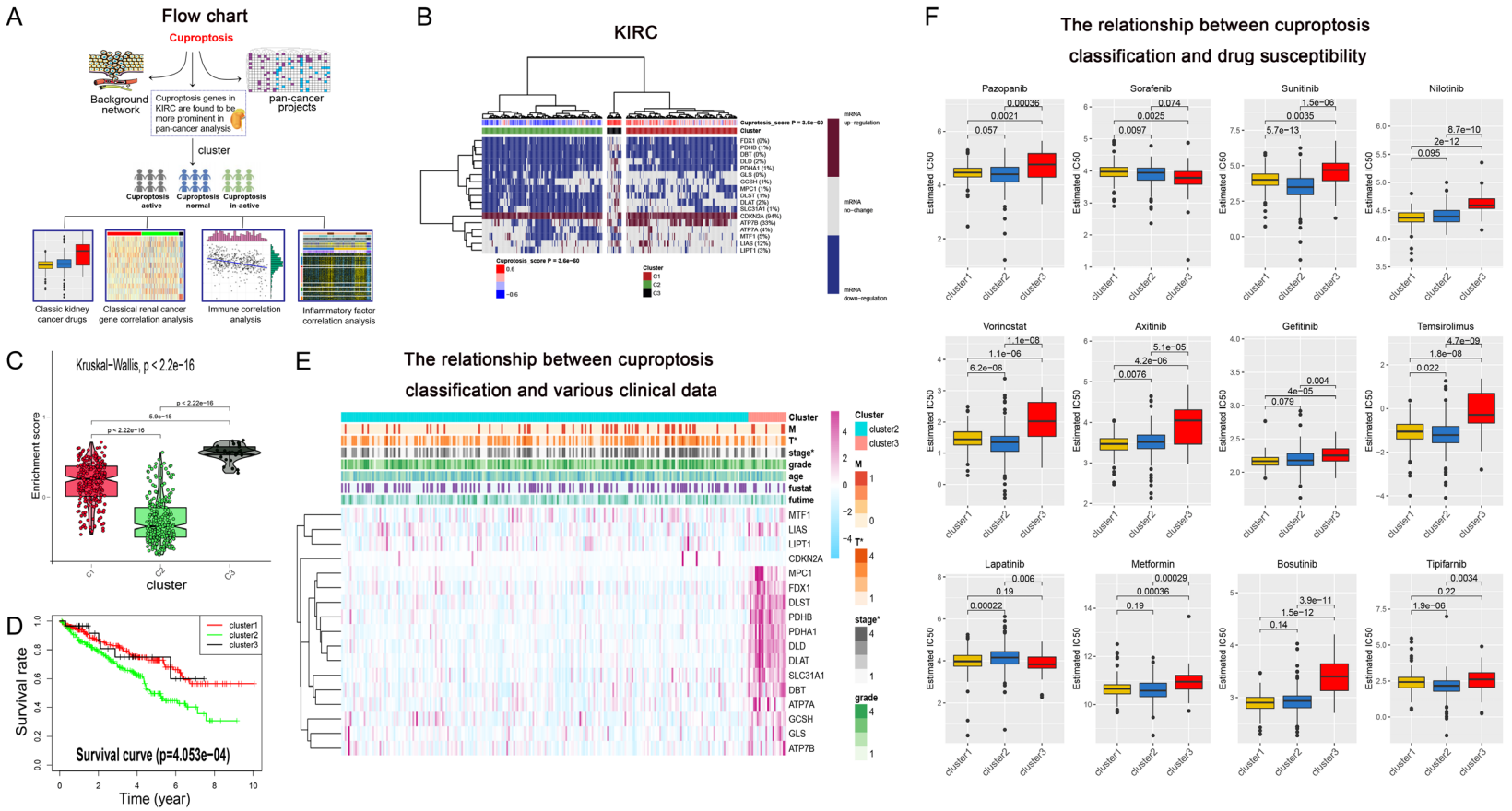

Figure 2. Cluster analysis and GDSC database. A. TCGA sample cohort was subjected to unsupervised clustering analysis based on the expression of cuprotosis-related genes, and the influence of the expression levels of cuprotosis-related genes on different clinical treatment hotspots in ccRCC was analyzed according to the three clusters obtained. The analysis was carried out from various perspectives such as classic drugs, classic oncogenes, immune infiltration and inflammatory factors. B. The heatmap shows the results of unsupervised clustering analysis, with red for up-regulated mRNA expression, grey for no difference in mRNA, and blue for down-regulated mRNA. The resulting three clusters are represented in red (no-change), green (inactive) and black (active), respectively. C. The violin plot shows the gene enrichment score for the three clusters. D. Survival curves for three cluster. E. The heatmap displays the gene expression of two clusters representing cuprotosis-active and cuprotosis-inactive, combined with tumor TNM stage (except for N), grade, age and survival. F. Based on the drug susceptibility test in GDSC, ridge regression was used to predict the drug susceptibility of three clusters to various classic anticancer drugs. Boxplots showing the prediction results.

showed obvious differences in the survival of the samples in these three clusters (**Figure 2C**, **2D**). These results validated our clustering analysis; hence, we performed subsequent correlation prediction analysis of cancer treatment on these three clusters. Using the two most distinct clusters Cluster2 and Cluster3, we integrated their clinicopathological features and genetic features in a heatmaps. As shown in **Figure 2E**, the degree of tumor invasion (T) and tumor stage in cluster3 (cuprotosis high expression) was significantly lower than those in cluster2 (cuprotosis low expression) ($P<0.05$). Meanwhile, we found that FDX1, DLAT, SLC31A1 and other cuprotosis-related genes were highly expressed in cluster3, which confirmed the authenticity of our cluster analysis and further indicated the correlation of cuprotosis with the inhibition of ccRCC and a better prognosis. The susceptibility test results of 12 different anticancer drugs in the three clusters were presented by boxplots. The data showed that Cluster2 and 3 had significantly different sensitivity to these drugs, and the results of most anti-cancer drugs showed a trend of change in the three clusters (**Figure 2F**). Furthermore, based on the previous survival analysis of the three clustered samples, we speculated that the differential expression of cuprotosis would affect the susceptibility to most targeted drugs. Indeed, there were significant differences in the sensitivity to the two commonly used drugs for renal cancer: axitinib [31] and sorafenib [32]. However, interestingly, the differences were not uniform. The samples with high cuprotosis expression were significantly more resistant to Axitinib, while they were less resistant to sorafenib. Similar differences were also observed to the rest of the common clinical drugs. It was noted that metformin [33], a NOVA drug with anticancer function, showed weak sensitivity to the samples with high expression of cupprotosis.

Clustering analysis of TCGA ccRCC samples and immunotherapy prediction analysis

Immunotherapy has been widely applied to ccRCC patients now, and the immune checkpoint inhibition therapy targeting programmed cell death protein 1/programmed cell death protein ligand 1 (PD-1/PD-L1) and cytotoxic t-lymphocyte-associated protein 4 (CTLA4) has become the standard treatment of ccRCC [34-36]. However, not all patients are sensitive to immunotherapy, and many ccRCC patients do not benefit from immunotherapy. Therefore, it is significant to stratify patients who will benefit from immunotherapy in clinical practice [37]. Hence, we sought to determine whether the difference in the expression of cuprotosis could be used for this purpose.

We first analyzed the degree of immune infiltration in ccRCC samples with differential expression of cuprotosis, and evaluated whether cuprotosis-related genes could be used to predict the outcomes of immunotherapy [38, 39]. We used the ssGSEA algorithm to obtain the expression levels of the marker genes of 24 immune cells in the TCGA ccRCC cohort samples and calculated the immune infiltration level of each sample. Finally, we obtained the correlation coefficient between the cuprotosis and the level of each immune infiltration indicator. The results were displayed in a balloon plot (**Figure 3A**). It showed that cuprotosis was negatively correlated with most of the immune infiltration indicators. Among them, Parainflammation and T-cell-co.stimulation, the two most prominent indicators, were selected, and their correlations with cuprotosis were independently displayed in scatter plots. **Figure 3B**, **3C** showed the clear negative correlation between these indicators and cuprotosis. Furthermore, we screened the genes involved in inflammatory factors in the samples of the

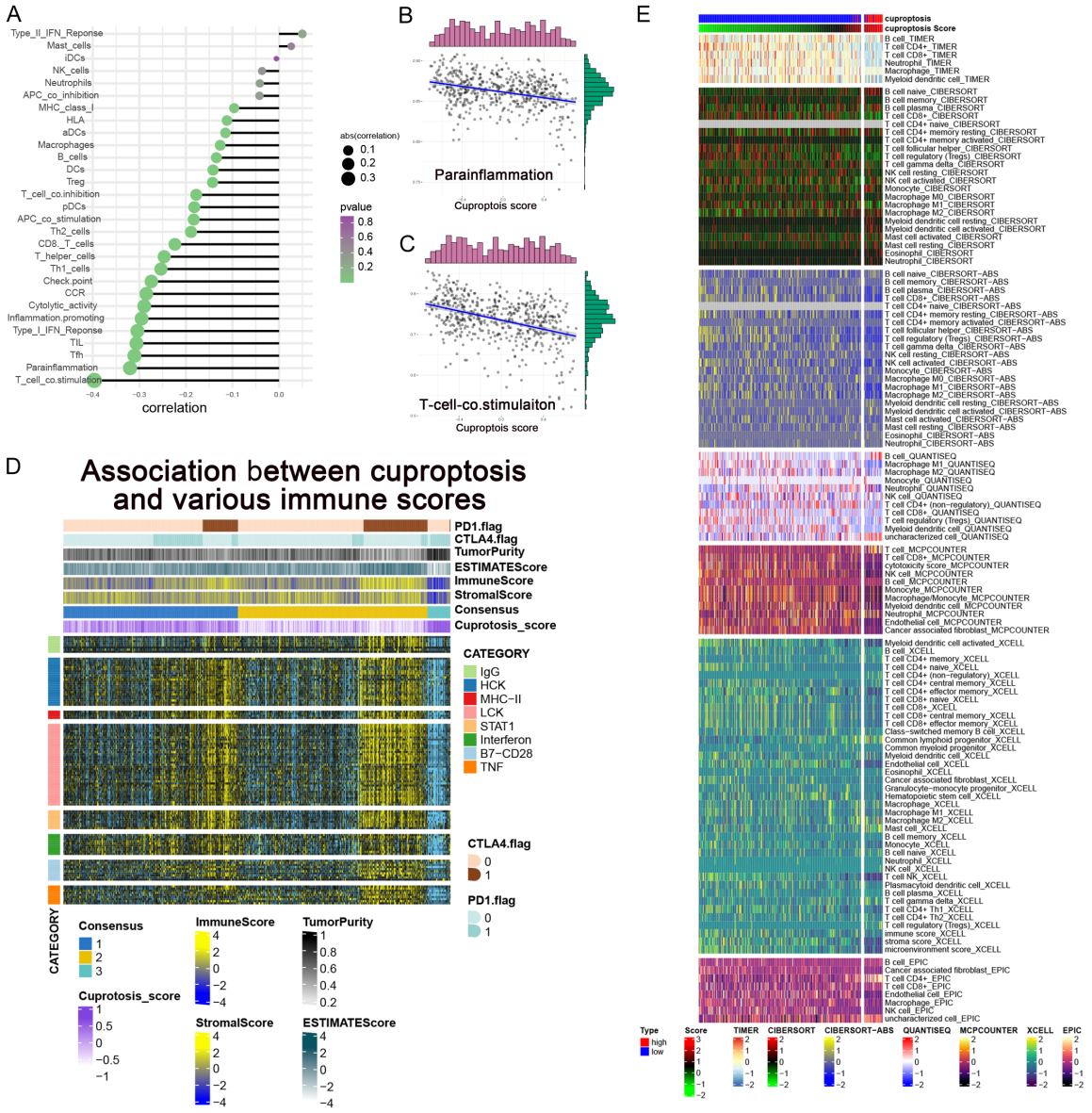

Figure 3. Immune infiltration analysis. A-C. Bubble plot shows the correlation between each immune infiltration index and cuprotosis. The two most correlated immune infiltration indicators: Parainflammation and T-cell-co.stimulation, and the correlation with cuprotosis is displayed in the form of scatter plot. D. Heatmap shows the gene expression levels of 8 inflammatory factors in different clusters, as well as the predictive results of 3 immune algorithm scores and responses to immune checkpoint inhibition therapy. The 8 inflammatory factors were: IgG, HCK, MHC-II, LCK, STAT1, Interferon, B7-CD28, TNF. E. Heatmap for immune responses based on different algorithms among the high and low-risk groups. Different algorithms are represented by different colored area bars.

TCGA ccRCC cohort and used a heat map to represent their differential expression levels compared to the normal cohort samples according to the three clusters. We selected seven key inflammatory factors in immunotherapy: IgG, HCK, LCK, MHC-II, STAT1, Interferon, B7-CD28 and TNF, as metagenes to cluster the genes in the TCGA database samples (**Figure 3D**). The results showed that higher expression of inflammatory factors was associated with higher immune score and lower cuprotosis score and was more likely to benefit from PD-1 and CTLA4 treatment.

Finally, we divided the TCGA ccRCC cohort samples into two groups: cuprotpsis-high and cuprotpsis-low, by using the best cut-off value according to the order of cuprotpsis score. Seven immune scoring algorithms, including TIMER, CIBERSORT, CIBERSORT-ABS,

QUANTISEQ, MCPCOUNTER, XCELL, and EPIC, were used to calculate and score the correlation between these samples and immune cells. The results obtained by these seven algorithms were integrated and displayed together with a heatmap (**Figure 3E**). The results suggested that higher cuprotosis score reflected a more negative correlation.

Clustering analysis of TCGA ccRCC samples and oncogenes and histone acetylation

We used a heatmap to show the expression of gene families associated with the canonical oncogene of ccRCC and histone acetylation related genes in different clusters (**Figure 4B**). We found that many canonical ccRCC oncogenes were altered along with the alteration in cuprotosis expression. For example, VHL [40-42] and mTOR [28, 43, 44], the two important molecules in oncogenic pathways in ccRCC, exhibited a significantly increased expression level with the increase of cuprotosis (Cluster2-Cluster3). In contrast, the expression level of MYC [45] and TP53 [46-48], the genes closely related to lipid metabolism in renal cancer, decreased significantly with the increased expression level of cuprotosis. Sirtuin (SIRT) and Histone Deacetylase (HDAC), the enzymes that regulate the acetylation and deacetylation of histone and non-histone targets [49], are known to play key roles in many physiological and pathological processes, including tissue homeostasis, maintenance of genomic stability, apoptosis, autophagy, senescence and tumorigenesis [50]. However, the function of SIRT and HDAC as tumor suppressors or tumor promoters is still not clear, and the favored notion is that both of them play a role in tumor tissues by affecting the balance between oxidative stress and DNA damage repair [51, 52]. Given that the functional mechanism of cuprotosis is closely related to oxidative stress in tumors, it is necessary to explore if the expression of SIRT family and HDAC family is correlated with the differential expression of cuprotosis.

Construction of prognostic models

After integrating the survival information of TCGA ccRCC cohort samples, we constructed a prognostic model based on cuprotosis-related gene expression in ccRCC patients (**Figure 4A**). Utilizing hazard analysis of the differential gene expression between the normal and the ccRCC cohorts, the *P* values and hazard ratio of 17 cuprotosis-related genes were calculated (**Figure 4C**, **4D**). The genes with P>0.05 were censored, and the remaining genes were analyzed by LASSO regression. At the end, 6 genes were utilized to construct the prognosis model (**Figure 4E**, **4F**). The risk score was the sum of the characteristic coefficients obtained by multiplying the expression of each gene in the sample by LASSO regression. The ccRCC cohort samples were divided into high-risk group and low-risk group after using the best cut-off value of risk score according to the algorithm (**Figure 4G-I**). Then, we used univariate COX regression and multivariate COX regression to construct the models for the samples in these two groups, respectively. The expression level of cuprotosis and the clinicopathological characteristics of the patients were integrated into the model construction. We found no significant difference in tumor TNM staging characteristics in the multivariate COX regression model (**Figure 4J**, **4K**). Finally, we constructed a prognostic model by integrating cuprotosis and the clinical characteristics of patients. The predicted AUC value of the model's 10-year survival rate was 0.729, which was acceptable for practical application (**Figure 4G**). The results were presented by nomogram (**Figure 4L**).

Validation with external data set

We validated our models with ArrayExpress and CPTAC databases at the transcriptional and protein levels, respectively (**Figure 5A**). Using the expression and survival information of Cuprotosis-related genes in samples from ArrayExpress, the survival curve was created based on the risk score and FDX1 (**Figure 5B**, **5C**). The survival curves showed that the prognosis of the high-risk group was significantly worse than that of the low-risk group, and the prognosis of the FDX1 high-expression group was significantly better than that of the low-expression group, which was consistent with our analysis with the TCGA cohort. The immunohistochemical results of cancer and paracancerous samples obtained from the CPTAC database indicated that the protein level of FDX1 was significantly lower in cancer samples than in paracancerous tissues, while CDKN2A protein level showed the opposite pattern (**Figure 5D-F**). Then the correlation-coefficient matrix of all genes are shown, and we also show the correlation between FDX1 and other genes. The results shows that there is a certain collinearity between these genes, and it is necessary to reduce the number of genes included in the model (**Figure 5G**, **5H**).

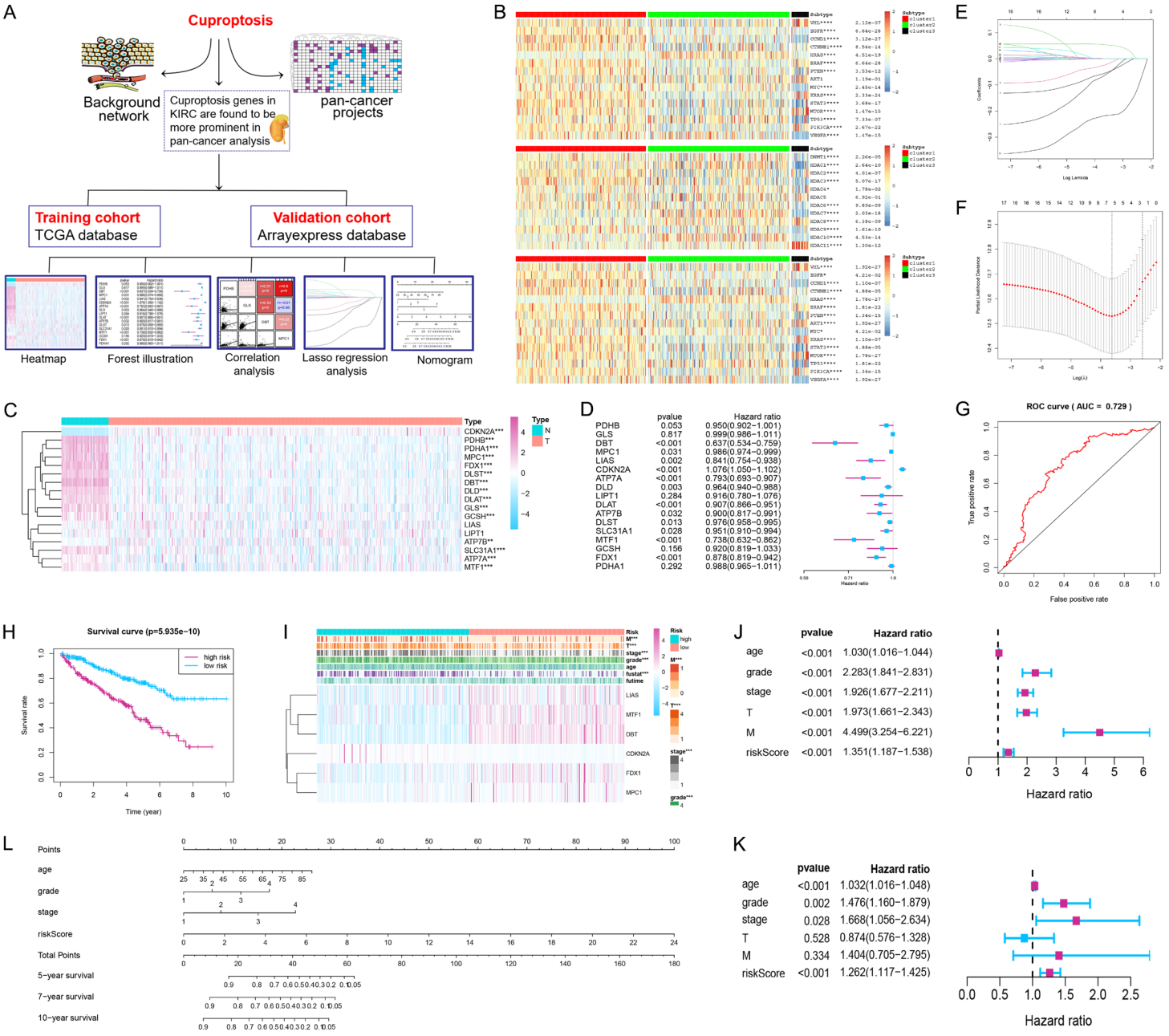
A
Cuproptosis
Background network
Cuproptosis genes in KIRC are found to be more prominent in pan-cancer analysis
pan-cancer projects
Training cohort
TCGA database
Validation cohort
Arrayexpress database
Heatmap
Forest illustration
Correlation analysis
Lasso regression analysis
Nomogram
B
C
D
pvalue
Hazard ratio
PDHB 0.053 0.950(0.902−1.001)
GLS 0.817 0.999(0.986−1.011)
DBT <0.001 0.637(0.534−0.759)
MPC1 0.031 0.986(0.974−0.999)
LIAS 0.002 0.841(0.754−0.938)
CDKN2A <0.001 1.076(1.050−1.102)
ATP7A <0.001 0.793(0.693−0.907)
DLD 0.003 0.964(0.940−0.988)
LIPT1 0.284 0.916(0.780−1.076)
DLAT <0.001 0.907(0.866−0.951)
ATP7B 0.032 0.900(0.817−0.991)
DLST 0.013 0.976(0.958−0.995)
SLC31A1 0.028 0.951(0.910−0.994)
MTF1 <0.001 0.738(0.632−0.862)
GCSH 0.156 0.920(0.819−1.033)
FDX1 <0.001 0.878(0.819−0.942)
PDHA1 0.292 0.988(0.965−1.011)
E
F
G
ROC curve (AUC = 0.729)
True positive rate
False positive rate
H
Survival curve (p=5.935e−10)
high risk
low risk
Survival rate
Time (year)
I
J
pvalue
Hazard ratio
age <0.001 1.030(1.016−1.044)
grade <0.001 2.283(1.841−2.831)
stage <0.001 1.926(1.677−2.211)
T <0.001 1.973(1.661−2.343)
M <0.001 4.499(3.254−6.221)
riskScore <0.001 1.351(1.187−1.538)
Hazard ratio
L
Points
age
grade
stage
riskScore
Total Points
5−year survival
7−year survival
10−year survival
K
pvalue
Hazard ratio
age <0.001 1.032(1.016−1.048)
grade 0.002 1.476(1.160−1.879)
stage 0.028 1.668(1.056−2.634)
T 0.528 0.874(0.576−1.328)
M 0.334 1.404(0.705−2.795)
riskScore <0.001 1.262(1.117−1.425)
Hazard ratio

Figure 4. Construction of clinical prognostic model. A. A cuprotosis-related prognostic model of ccRCC patients was constructed by combining the gene expression data in the TCGA cohort samples with the clinical and pathological characteristics data for analysis. B. The heat map shows the gene expression of canonical oncogenes of ccRCC, HDAC family, and SIRT family in the three clustered samples, respectively. C. Comparison of the expression of cuprotosis-related genes between cancer tissue cohorts and normal tissue cohorts in the TCGA database. D. The forest plot shows the Hazard ratio value and *P* value of each cuprotosis-related gene after COX regression analysis. E, F. 6 genes were screened from 17 cuprotosis-related genes by LASSO regression as risk-score features for building survival prediction models. G. ROC curve of the 10-year survival prediction model constructed based on cuprotosis-related genes and features of clinical and pathological. H. Survival curves of high-risk and low-risk groups adjudicated with the median as the cutoff. I. The heat map shows the comparison of the clinical characteristics, pathological characteristics, and expression levels of the six genes screened by LASSO regression between the high-risk group and the low-risk group. J. The Hazard ratio and *P* value of each feature used to construct the survival prediction model were calculated by univariate COX regression. K. The Hazard ratio and *P* value of each feature used to construct the survival prediction model were calculated by multivariate COX regression. L. Display the resulting predictive model with a Nomogram.

Finally, by using the radiomics analysis, we evaluated the predictive value of the expression of cuprotosis in patients by using 75 samples with perfect CT image data corresponding to the TCGA samples selected from TCIA. We classified these 75 samples according to the results of cluster analysis and extracted radiomic features. After screening, the information of 10 radiomics features was obtained (**Figure 5I-L**). Five machine learning classifiers were used to build the prediction model, and the prediction model by the four classifier algorithms, Support Vector Machine (SVM), LightGBM, Random Forest (RF), and Xgboost showed better performance. The AUCs were all greater than 0.7 (**Figure 5M-Q**), suggesting the feasibility of using CT imaging characteristics and the gene expression of Cuprotosis to guide treatment option.

Tumor mutational burden

Tumor mutational burden (TMB) was defined as the total number of somatic gene coding errors, base substitutions, and gene insertion or deletion errors detected per megabase [36]. TMB is a new marker for evaluating the therapeutic effect of PD-1/PD-L1 and CTLA-4, and its effect has been confirmed in the treatment of colorectal cancer with mismatch repair deficiency [53, 54] (**Figure 6**). Since PD-1/PD-L1 inhibitors have been widely used in the treatment of ccRCC [35, 37, 38], it will be significant to apply TMB to evaluate the benefit of ccRCC patients receiving PD-1/PD-L1 therapy. After calculating the TMB value for each sample, we found that the TMB value was higher in the high-risk group than in the low-risk group. Next, we divided the high- and low-risk groups into 4 subgroups according to the TMB value, and the survival curve showed that the prognosis of the high TMB group was significantly better than that of the low TMB group, suggesting that TMB value was significantly correlated with the prognosis of ccRCC patients. Hence, combining cuprotosis and TMB as indicators to evaluate the benefit of PD-1/PD-L1 inhibitor therapy in patients will be more precise and reliable. We displayed the TMB down to the mutational profile of a single gene as a heatmap, and the results showed that, in addition to the frequently mutated genes VHL and PBRM1 in renal cancer, mutations in SETD2 and TTN were common too. Recent studies have shown that SETD2 induces the down-regulation of FBW7 expression and promotes NFAT1 degradation in sunitinib-resistant RCC, suggesting that SETD2 contributes to the regulation of the immune response in RCC [55]. TNN mutation has been found in the immune microenvironment of bladder cancer and colon cancer and is closely related to prognosis [56, 57]. Since there are only few studies about TTN mutation in the treatment of ccRCC, our results provide a new insight into the immunotherapy of ccRCC.

Discussion

With the advancement in the understanding of renal cancer, the clinical treatment of ccRCC has developed from radiotherapy and chemotherapy, which have poor sensitivity and specificity, to targeted therapy, immunotherapy and other more precision treatments [31, 32, 40, 58]. These therapies inhibit the proliferation and metastasis of ccRCC cancer cells by affecting the expression levels of genes in signaling pathways involved in proliferation, metastasis, death, and the prognosis of ccRCC. How to regulate the expression of key genes in these

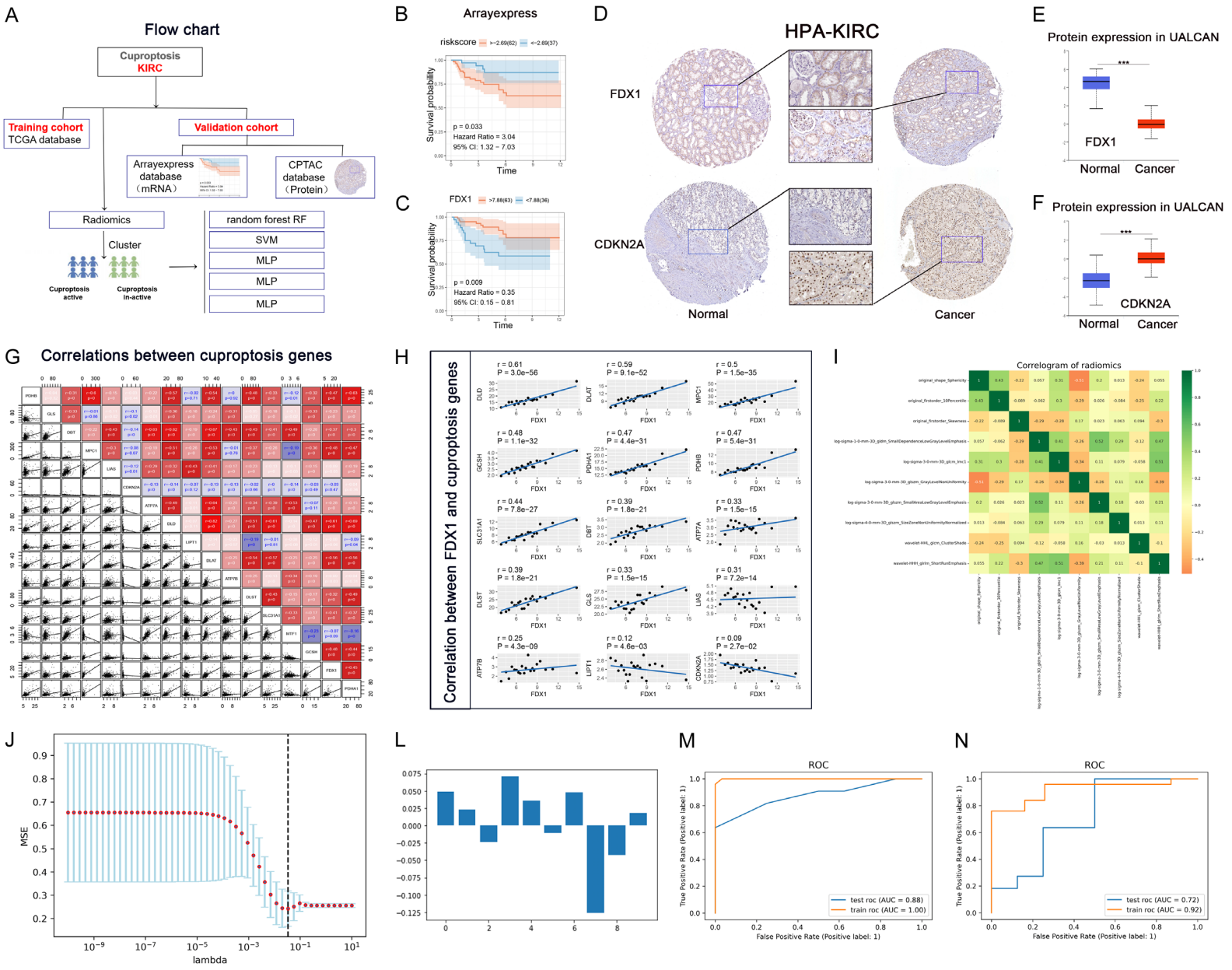
A
Flow chart
Cuproptosis KIRC
Training cohort TCGA database
Validation cohort
Arrayexpress database (mRNA)
CPTAC database (Protein)
Radiomics
Cluster
Cuproptosis active
Cuproptosis in-active
random forest RF
SVM
MLP
MLP
MLP
B
Arrayexpress
riskscore
Survival probability
p = 0.033
Hazard Ratio = 3.04
95% CI: 1.32 ~ 7.03
Time
C
FDX1
Survival probability
p = 0.009
Hazard Ratio = 0.35
95% CI: 0.15 ~ 0.81
Time
D
HPA-KIRC
FDX1
CDKN2A
Normal
Cancer
E
Protein expression in UALCAN
FDX1
Normal
Cancer
F
Protein expression in UALCAN
CDKN2A
Normal
Cancer
G
Correlations between cuproptosis genes
H
Correlation between FDX1 and cuproptosis genes
I
Correlogram of radiomics
J
MSE
lambda
L
M
ROC
True Positive Rate (Positive label: 1)
False Positive Rate (Positive label: 1)
test roc (AUC = 0.88)
train roc (AUC = 1.00)
N
ROC
True Positive Rate (Positive label: 1)
False Positive Rate (Positive label: 1)
test roc (AUC = 0.72)
train roc (AUC = 0.92)

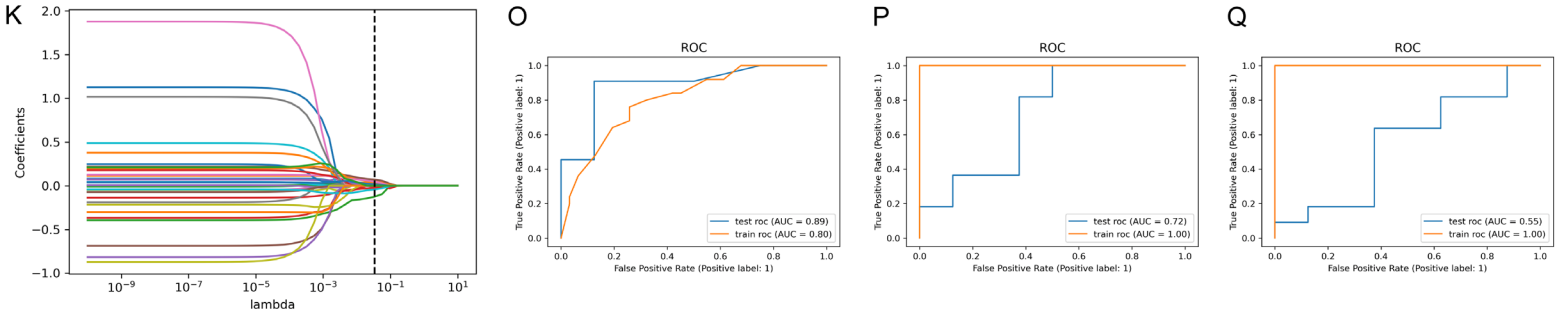

Figure 5. External data validation. A. Two external data, Arrayexpress and CPTAC, were used to verify the analysis results of the TCGA database, and the CT images in the TCIA image database were collected to find suitable imaging features, and a variety of model building methods in machine learning were used to construct the prediction model of expression subtypes of cuprotosis. B, C. Using the Arrayexpress database to verify the results of the TCGA database from two levels: the macroscopic-cuprotosis-related gene set and the microscopic-FDX1 single gene. Differences in results are shown with survival curves. D. The CPTAC database was used to verify the protein expression of FDX1 and CDKN2A in tumor tissue and normal tissue from the proteomic level. The images show the immunohistochemical (IHC) results of cancer tissue and normal tissue. E, F. The protein expression levels in the CPTAC database were retrieved from UALCAN to show the comparison between tumor tissue and normal tissue. G, H. Correlations among the 17 cuprotosis-related genes are shown in the heatmap. The correlation of FDX1 with other cuprotosis-related genes is additionally represented. I, J. Feature screening using LASSO regression to get 10 radiomics features. K. Heatmap showing the correlation between 10 radiomics features filtered by t-test and LASSO regression. L. The weights of the 10 radiomics features, corresponding from 1 to 10: 1.original_shape_Sphericity, 2.orginal_firstorder_10Percentile, 3.original_firstorder_Skewness, 4.log-sigma-1-0-mm-3D_gldm_SmallDependenceLowGrayLevelEmphasis, 5.log-sigma-3-0-mm-3D_glcm_Imc1, 6.log-sigma-3-0-mm-3D_glszm_GrayLevelNonUniformity, 7.log-sigma-3-0-mm-3D_glszm_SmallAreaLowGrayLevelEmphasis, 8.log-sigma-4-0-mm-3D_glszm_SizeZoneNonUniformityNormalized, 9.wavelet-HHL_glcm_ClusterShade, 10.wavelet-HHH_glrlm_shortRunEmphasis. M-Q. Based on 10 selected radiomics features, five machine learning strategies of RF, SVM, MLP, XGboost and lightgbm are used to build a prediction model.

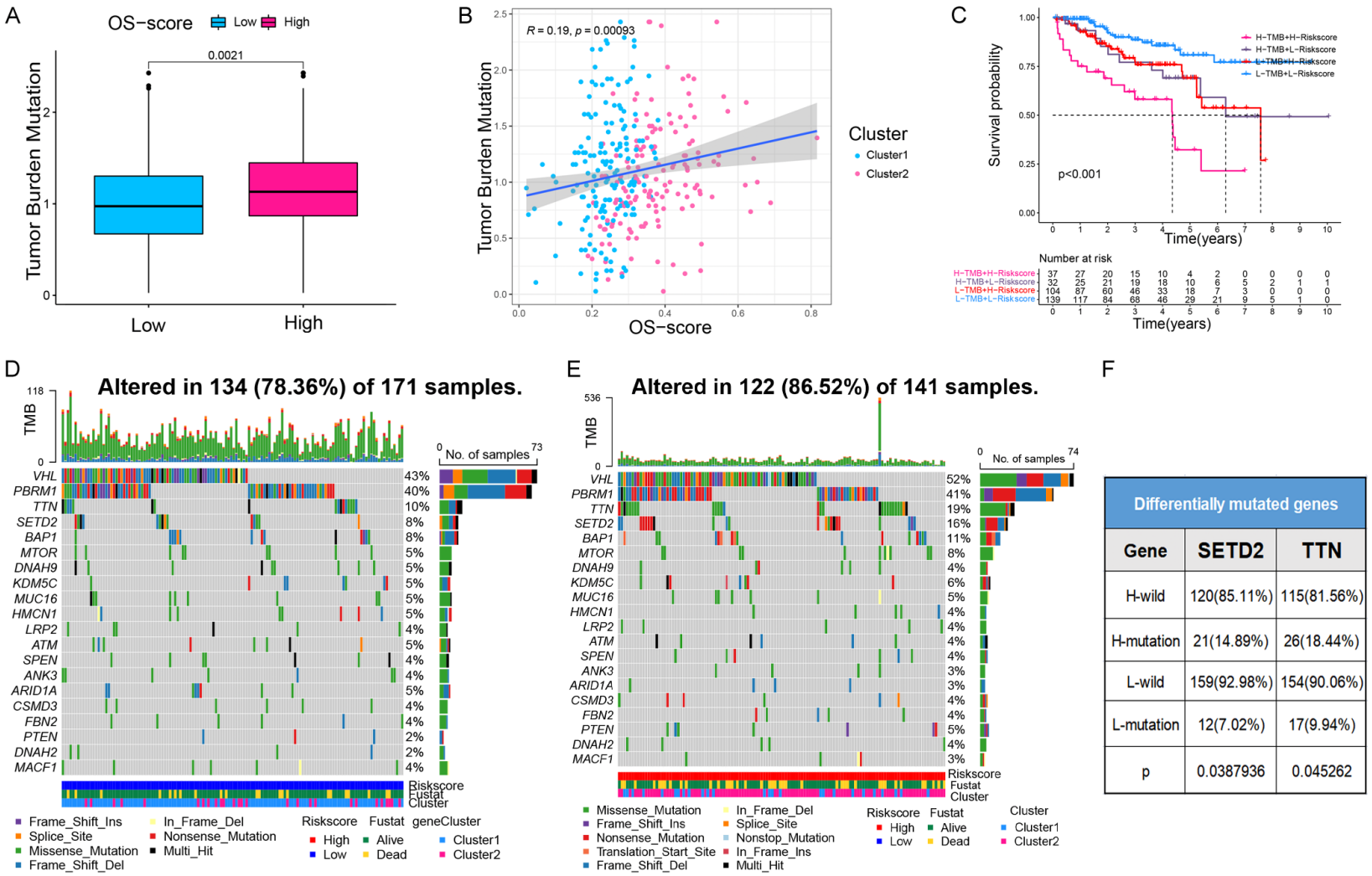

F

Differentially mutated genes		
Gene	SETD2	TTN
H-wild	120(85.11%)	115(81.56%)
H-mutation	21(14.89%)	26(18.44%)
L-wild	159(92.98%)	154(90.06%)
L-mutation	12(7.02%)	17(9.94%)
p	0.0387936	0.045262

Figure 6. Tumor burden mutation. A. Comparison of tumor burden mutation based on high and low risk groups. B. Scatter plots show the correlation between tumor mutations burden and riskscore. C. Survival curve of sample grouping after comprehensive consideration of tumor mutation burden and riskscore. D, E. Two heatmaps show tumor mutational burden in high and low risk groups, respectively. F. Figure shows eigenvalues of tumor mutational burden for SETD2 and TTN.

important pathways has become the focus of clinical treatment of ccRCC.

Regulatory cell death (RCD) is a gene-regulated mode of cell death [59]. Based on the differences in signaling pathways, RCD can be classified into different types, including apoptosis, the first discovered RCD, necroptosis, autophagy, ferroptosis, pyroptosis, and cuprotosis [60-62]. Numerous studies have shown that the excessive accumulation of copper ions can produce cytotoxicity, and increasing the intracellular copper ion concentration can achieve specific killing effect in cancer cells [63]. Cuprotosis is a newly discovered form of regulatory cell death caused by the excessive accumulation of copper ions, thereby leading to the destruction of certain mitochondrial metabolic enzymes and cell death [2]. Specifically, if the lipidylation level of TCA-related enzymes is increased, the modified proteins will directly bind to copper ion and aggregate, leading to the loss of Fe-S cluster-containing proteins and the activation of HSP70, which further results in acute proteolytic toxic stress [64]. In addition, it is also found that FDX1, a key regulatory gene for cuprotosis, is associated with the synthesis of Fe-S cluster-containing proteins [65]. Hence, from our and other studies, it is evident that the occurrence and progression of kidney cancer are closely related to the reprogramming of lipid metabolism [10, 66-68]. Given the close relationship between cuprotosis and TCA, we proposed that cuprotosis could be a potential target for the treatment of kidney cancer, which warrants further investigations. Several lines of evidence support this notion; for example, significant changes in copper content in the serum and the tumor tissues of cancer patients have been reported. In addition to FDX1 regulation of cuprotosis, copper ions is also related to vascular endothelial growth factor (VEGF) and fibroblast growth factor (FGF1) [69, 70]. Furthermore, a recent clinical trial showed that copper ion was related to the stability of HIF-1, an important regulatory gene in the metabolism of ccRCC [71]. Considering the importance of warburg effect, our findings of the link between copper ions and TCA further highlighted the potential clinical application of cuprotosis [72].

Since the role of cuprotosis in cancer is still not fully understood, we performed a pan-cancer analysis of cuprotosis-related genes based on the gene expression data of 33 cancer samples from TCGA. The results indicated that cuprotosis played a diverse role in various cancers (**Figure 1**). For example, cuprotosis was a risk factor in liver cancer and prostate cancer, while it had a risk and protective effect in mesothelioma and adrenal cortical cancer. In ccRCC, we found that most cuprotosis related genes were differentially expressed compared to normal tissues, and that cuprotosis had protection role in most cases. These results are exciting and suggest the potential of cuprotosis in ccRCC targeted therapy. To further categorize the subtypes of differential expression of cuprotosis in TCGA ccRCC cohort, we applied unsupervised cluster analysis. Compared with normal cohort, the ccRCC cohort was divided into three clusters based on the expression level of cuprotosis. Statistical analysis indicated that there were significant differences among these clusters.

Since many drugs have been developed for the clinical treatment of ccRCC, we analyzed the effect of differential expression of cuprotosis on the sensitivity of ccRCC samples to these common drugs. We selected 12 drugs from GDSC database that are first-line or second-line drugs in the treatment of renal cancer [73]. The IC50 prediction of these drugs showed that the IC50 of almost all drugs was significant different between the high and low cuprotosis expression groups, and most drugs had the same trend of either increasing or decreasing in IC50 values in each group. This result suggested that the efficacy of all the commonly used ccRCC drugs might be related to cuprotosis and that the differential expression of cuprotosis could be used to guide the treatment selection. Therefore, we further explored the prediction value of cuprotosis-related gene expression combined with current highly recognized treatment plans in the treatment of ccRCC patients. Since PD-1/PD-L1 inhibitors are the new immunotherapeutic approach widely used in the treatment of ccRCC [38], we examined whether cuprotosis could affect the outcomes of immunotherapy in ccRCC. Using ssGSEA algorithm [74], we analyzed the degree of immune infiltration of each ccRCC sample and calculated the immune score of samples with different cuprotosis expression levels as well as the responsiveness and benefits of PD-1/CTLA4. The correlation analysis results

showed that most immune infiltrating cells were inversely correlated with cuprotosis expression, and the response to PD-1 treatment in the low cuprotosis expression group was significantly better than that in the high cuprotosis expression group, while CTLA-4 showed the opposite pattern, suggesting that cuprotosis could guide the use of immunotherapy in patients with ccRCC, and that the combination of cuprotosis-targeted therapy and immunotherapy had clinical therapeutic value. To further explore the functional mechanism of cuprotosis in ccRCC, we investigated the relationship between cuprotosis and oncogene and histone modification. We found that many oncogenes, such as VHL, EGFR, MYC and P53, were expressed differentially in different cuprotosis expression groups [41, 48, 75]. Moreover, the two major histone acetylation and deacetylatation enzymes, SIRT and HDAC, also has a significant correlation with the differential expression of cuprotosis. Hence, our study provided rationale for targeting cuprotosis-related genes in clinical treatment.

Using the patient survival information in the TCGA database, we constructed a cuprotosis-related genes-based prognostic model. We further integrated the patient's age, stage, grade, and pathological information into the model construction. After feature screening by univariate and multivariate COX regression and LASSO regression, we constructed a patient prognosis model by logistic regression. Compared with other prognostic model construction methods, our prognostic model had many advantages and innovations. First, LASSO regression was used to force the gene coefficient with low correlation to 0, which reduced the dimension of data matrix, avoided the occurrence of dimension disaster, and reduced the algorithm burden of model construction in the later stage. Second, dimensionality reduction helped remove noise from sample data, reduced overfitting, and increased the authenticity of the model; meanwhile, it also provided valuable information. The genes screened out could be considered as the key genes for the function of cuprotosis in ccRCC. Of the six genes identified, FDX1 and LIAS have been shown to be important in the cuprotosis signaling pathway. Another gene, metal-regulated transcription factor 1 (MTF1), is a conserved metal-binding transcription factor in eukaryotes that binds to conserved DNA motifs and is known as a metal reaction element [76]. MTF1 responds to changes in the body's metal content, protects cells from oxidative and hypoxia stress, and is essential for vertebrate embryonic development. MTF1 has been shown to be down-regulated in ferroptosis in cancer, eliminate the serine/threonine kinase ATM (mutated in ataxia-telangiatosis) regulation of iron regulatory elements, and re-sensitize cells to iron apoptosis, which helps the targeted therapy of cancer cells [77]. Therefore, we speculated that MTF1 might play a similar role in cuprotosis, and that MTF1 might serve as a potential therapeutic target. The other three genes, DBT, CDKN2A and MPC1, have not been reported to have effects on copper metabolism or in the proliferation and metastasis of ccRCC cells or other cancer cells. Further verification is needed. Moreover, by calculating the correlation among genes, we found that these 6 genes were highly independent, which was conducive to the construction of the model. The 10-year AUC area value of the test set and the verification results of the external database ArrayExpress and CPTAC suggested that our model had good reliability and could be used in the survival prediction of ccRCC patients.

Sequencing of targeted gene expression and mutations (CNV, SNV, et al.) of patients and evaluating the response and benefit of patients receiving certain targeted drugs or immune drugs are currently the important standard in guiding therapy options for ccRCC and other cancer patients [78]. However, due to the high demand in technology and the high cost of this method, its application is limited in developing countries. Therefore, we aimed to find alternatives of genetic testing to remedy the above limitations. We focused our study on radiomics. After examining the ccRCC related radiomics data, we used multiple prediction models based on machine learning to determine the cuprotosis expression level in patients by searching for the differential features of CT images of samples with differential expression of cuprotosis [79, 80]. Our initial goal was to have prediction models with high predictive power (AUC>0.9); however, the results were not ideal, and only the Random Forest model barely reached about 0.8 AUC. Prediction of cuprotosis expression based on CT images of patients was one of our attempts, and the research of

Radiomics was not in-depth. Although the results did not reach the ideal level, we hope to find more methods to replace or combine genetic testing to obtain relatively accurate treatment guidelines for patients at a lower cost. In addition to radiomics, we also evaluated the effect of PD-1 inhibitor therapy by calculating TMB levels in ccRCC samples. TMB generally refers to the number of non-synonymous mutations of somatic cells in a specific region, and its evaluation results are affected by sample quality, tested genome size, and bioinformation analysis methods. TMB value can reflect the potential of tumor neoantigen production in tumor and is closely related to DNA repair defects [81]. Studies have shown lower survival in patients with higher TMB, but the opposite is true in patients treated with immune checkpoint suppression as patients with higher TMB generally have longer survival [82]. In our study, the expression level and coefficient of cuprotosis-related genes screened by LASSO regression were also calculated, and the risk-score of each sample was calculated. Next, the optimal cut-off value was used to divide all samples into high-risk group and low-risk group. Based on the risk score of these two groups and the level of TMB, we divided the high-risk group and the low-risk group into four groups: high risk - high TMB, high risk - low TMB, low risk - high TMB and low risk - low TMB. By analyzing their survival, we found that TMB was indeed correlated with the prognosis of patients, and the prognosis of patients with high TMB was poor. In addition, the combination of TMB value and cuprotosis expression level could better distinguish different subgroups, indicating the response of cuprotosis to immune checkpoint inhibition therapy and the ability to predict the prognosis of patients. Currently, cuprotosis has not been used to determine the benefit of immune checkpoint inhibition in ccRCC patients; hence, our results may provide a rationale for further investigation.

Our results have been proven to be reliable through multiple verifications, such as verification by protein expression level, external gene set, and radiomic data. However, this study lacks the support from experimental data. Since the mechanism of cuprotosis has not been fully determined, more experimental results will be important to validate the bioinformatics analysis results. Further investigation on the new RCD mechanism of cuprotosis will be critical for the clinical application of cuprotosis in the treatment of cancer or other common diseases.

Acknowledgements

We are very grateful to the TCGA database and the TCIA database for the gene expression information and image information provided to our samples. We thank Prof. Che and Prof. Wang for providing us with the necessary hardware facilities for computational analysis. The PhD Start-up Fund of Liaoning Province from GW (2021-BS-209, Liaoning Province, 30000 CNY). Dalian Youth Science and Technology Star from GW (2021RQ010, Dalian, 100000CNY).

Disclosure of conflict of interest

None.

Abbreviation

ccRCC/KIRC, Kidney renal clear cell carcinoma; RCD, Regulatory cell death; CDKN2A, Cyclin-dependent kinase inhibitor 2a; DBT, Dihydrolipoamide branched chain Transacylase E2; PDHB, Pyruvate dehydrogenase E1 subunit beta; GLS, Glutaminase; MPC1, Mitochondrial pyruvate carrier 1; LIAS, Lipoic acid synthetase; ATP7A, ATPase copper transporting alpha; DLD, Dihydrolipoamide Dehydrogenase; LIPT1, Lipoyltransferase 1; DLAT, Dihydrolipoamide S-acetyltransferase; ATP7B, ATPase copper transporting beta; DLST, Dihydrolipoamide S-succinyltransferase; SLC31A1, Solute carrier family 31 member 1; MTF1, Metal regulatory transcription factor 1; GCSH, Glycine cleavage system protein H; FDX1, Ferredoxin 1; PDHA1, Pyruvate dehydrogenase E1 subunit alpha 1; PD-1/PD-L1, Programmed cell death protein 1/programmed cell death ligand 1; CNV, Copy number variation; SNV, Single nucleotide variant; LASSO, Least absolute shrinkage and selection operator; GSEA, Gene set enrichment analysis; HDAC, Histone deacetylase; SIRT, Sirtuin; CTLA4, Cytotoxic T-lymphocyte antigen-4; TMB, Tumor mutational burden; ACC, Adrenocortical carcinoma; BLCA, Bladder Urothelial Carcinoma; BRCA, Breast invasive carcinoma; CESC, Cervical squamous cell carcinoma and endocervical adenocarcinoma; CHOL, Cholangiocarcinoma; DLBC, Lymphoid neoplasm diffuse large B-cell lymphoma; ESCA,

Esophageal carcinoma; GBM, Glioblastoma multiforme; HNSC, Head and neck squamous cell carcinoma; KICH, Kidney chromophobe; KIRP, Kidney renal papillary cell carcinoma; LAML, Acute myeloid leukemia; LGG, Brain lower grade glioma; LIHC, Liver hepatocellular carcinoma; LUAD, Lung adenocarcinoma; LUSC, Lung squamous cell carcinoma; MESO, Mesothelioma; OV, Ovarian serous cystadenocarcinoma; PAAD, Pancreatic adenocarcinoma; PCPG, Pheochromocytoma and paraganglioma; PRAD, Prostate adenocarcinoma; READ, Rectum adenocarcinoma; STAD, Stomach adenocarcinoma; STES, Stomach and esophageal carcinoma; UCS, Uterine carcinosarcoma; UVM, Uveal melanoma; THCA, Thyroid carcinoma; THYM, Thymoma; UCEC, Uterine ccorpus endometrial carcinoma; SKCM, Skin cutaneous melanoma; COAD, Colon adenocarcinoma.

Address correspondence to: Guangzhen Wu and Qifei Wang, Department of Urology, The First Affiliated Hospital of Dalian Medical University, No. 222 Zhongshan Road, Dalian 116011, Liaoning, China. Tel: +86-18098876012; E-mail: wuguangzhen@firsthosp-dmu.com (GZW); Tel: +86-18098876008; E-mail: wangqifei6008@hotmail.com (QFW)

References

[1] Ge EJ, Bush AI, Casini A, Cobine PA, Cross JR, DeNicola GM, Dou QP, Franz KJ, Gohil VM, Gupta S, Kaler SG, Lutsenko S, Mittal V, Petris MJ, Polishchuk R, Ralle M, Schilsky ML, Tonks NK, Vahdat LT, Van Aelst L, Xi D, Yuan P, Brady DC and Chang CJ. Connecting copper and cancer: from transition metal signalling to metalloplasia. Nat Rev Cancer 2022; 22: 102-113.

[2] Tsvetkov P, Coy S, Petrova B, Dreishpoon M, Verma A, Abdusamad M, Rossen J, Joesch-Cohen L, Humeidi R, Spangler RD, Eaton JK, Frenkel E, Kocak M, Corsello SM, Lutsenko S, Kanarek N, Santagata S and Golub TR. Copper induces cell death by targeting lipoylated TCA cycle proteins. Science 2022; 375: 1254-1261.

[3] Lopez-Beltran A, Carrasco JC, Cheng L, Scarpelli M, Kirkali Z and Montironi R. 2009 update on the classification of renal epithelial tumors in adults. Int J Urol 2009; 16: 432-43.

[4] Siegel RL, Miller KD and Jemal A. Cancer statistics, 2020. CA Cancer J Clin 2020; 70: 7-30.

[5] Guo H, Jiang S, Sun H, Shi B, Li Y, Zhou N, Zhang D and Guo H. Identification of IL20RB as a novel prognostic and therapeutic biomarker in clear cell renal cell carcinoma. Dis Markers 2022; 2022: 9443407.

[6] Zou Y, Henry WS, Ricq EL, Graham ET, Phadnis VV, Maretich P, Paradkar S, Boehnke N, Deik AA, Reinhardt F, Eaton JK, Ferguson B, Wang W, Fairman J, Keys HR, Dančík V, Clish CB, Clemons PA, Hammond PT, Boyer LA, Weinberg RA and Schreiber SL. Plasticity of ether lipids promotes ferroptosis susceptibility and evasion. Nature 2020; 585: 603-608.

[7] Wu G, Zhang Z, Tang Q, Liu L, Liu W, Li Q and Wang Q. Study of FABP's interactome and detecting new molecular targets in clear cell renal cell carcinoma. J Cell Physiol 2020; 235: 3776-3789.

[8] Hilgendorf KI, Johnson CT, Mezger A, Rice SL, Norris AM, Demeter J, Greenleaf WJ, Reiter JF, Kopinke D and Jackson PK. Omega-3 fatty acids activate ciliary ffar4 to control adipogenesis. Cell 2019; 179: 1289-1305, e21.

[9] Wu G, Xu Y, Wang Q, Li J, Li L, Han C and Xia Q. FABP5 is correlated with poor prognosis and promotes tumour cell growth and metastasis in clear cell renal cell carcinoma. Eur J Pharmacol 2019; 862: 172637.

[10] Wu G, Wang Q, Xu Y, Li J, Zhang H, Qi G and Xia Q. Targeting the transcription factor receptor LXR to treat clear cell renal cell carcinoma: agonist or inverse agonist? Cell Death Dis 2019; 10: 416.

[11] Zanfardino M, Pane K, Mirabelli P, Salvatore M and Franzese M. TCGA-TCIA impact on radiogenomics cancer research: a systematic review. Int J Mol Sci 2019; 20: 6033.

[12] van Griethuysen JJM, Fedorov A, Parmar C, Hosny A, Aucoin N, Narayan V, Beets-Tan RGH, Fillion-Robin JC, Pieper S and Aerts HJWL. Computational radiomics system to decode the radiographic phenotype. Cancer Res 2017; 77: e104-e107.

[13] Tomczak K, Czerwińska P and Wiznerowicz M. The cancer genome atlas (TCGA): an immeasurable source of knowledge. Contemp Oncol (Pozn) 2015; 19: A68-77.

[14] Parkinson H, Sarkans U, Shojatalab M, Abeygunawardena N, Contrino S, Coulson R, Farne A, Lara GG, Holloway E, Kapushesky M, Lilja P, Mukherjee G, Oezcimen A, Rayner T, Rocca-Serra P, Sharma A, Sansone S and Brazma A. ArrayExpress--a public repository for microarray gene expression data at the EBI. Nucleic Acids Res 2005; 33: D553-5.

[15] Yang W, Soares J, Greninger P, Edelman EJ, Lightfoot H, Forbes S, Bindal N, Beare D, Smith JA, Thompson IR, Ramaswamy S, Futreal PA, Haber DA, Stratton MR, Benes C, McDermott U and Garnett MJ. Genomics of drug sensitivity in cancer (GDSC): a resource for therapeutic biomarker discovery in cancer cells. Nucleic Acids Res 2013; 41: D955-61.

[16] Edwards NJ, Oberti M, Thangudu RR, Cai S, McGarvey PB, Jacob S, Madhavan S and Ketchum KA. The CPTAC data portal: a resource for cancer proteomics research. J Proteome Res 2015; 14: 2707-13.
[17] Prior FW, Clark K, Commean P, Freymann J, Jaffe C, Kirby J, Moore S, Smith K, Tarbox L, Vendt B and Marquez G. TCIA: an information resource to enable open science. Annu Int Conf IEEE Eng Med Biol Soc 2013; 2013: 1282-5.
[18] Hänzelmann S, Castelo R and Guinney J. GSVA: gene set variation analysis for microarray and RNA-seq data. BMC Bioinformatics 2013; 14: 7.
[19] Chen J, Zaidi S, Rao S, Chen JS, Phan L, Farci P, Su X, Shetty K, White J, Zamboni F, Wu X, Rashid A, Pattabiraman N, Mazumder R, Horvath A, Wu RC, Li S, Xiao C, Deng CX, Wheeler DA, Mishra B, Akbani R and Mishra L. Analysis of genomes and transcriptomes of hepatocellular carcinomas identifies mutations and gene expression changes in the transforming growth factor-β pathway. Gastroenterology 2018; 154: 195-210.
[20] Lu X, Jiang L, Zhang L, Zhu Y, Hu W, Wang J, Ruan X, Xu Z, Meng X, Gao J, Su X and Yan F. Immune signature-based subtypes of cervical squamous cell carcinoma tightly associated with human papillomavirus type 16 expression, molecular features, and clinical outcome. Neoplasia 2019; 21: 591-601.
[21] Finotello F and Trajanoski Z. Quantifying tumor-infiltrating immune cells from transcriptomics data. Cancer Immunology Immunotherapy 2018; 67: 1031-1040.
[22] Tardito S, Bassanetti I, Bignardi C, Elviri L, Tegoni M, Mucchino C, Bussolati O, Franchi-Gazzola R and Marchiò L. Copper binding agents acting as copper ionophores lead to caspase inhibition and paraptotic cell death in human cancer cells. J Am Chem Soc 2011; 133: 6235-42.
[23] Cui L, Gouw AM, LaGory EL, Guo S, Attarwala N, Tang Y, Qi J, Chen YS, Gao Z, Casey KM, Bazhin AA, Chen M, Hu L, Xie J, Fang M, Zhang C, Zhu Q, Wang Z, Giaccia AJ, Gambhir SS, Zhu W, Felsher DW, Pegram MD, Goun EA, Le A and Rao J. Mitochondrial copper depletion suppresses triple-negative breast cancer in mice. Nat Biotechnol 2021; 39: 357-367.
[24] Hasinoff BB, Yadav AA, Patel D and Wu X. The cytotoxicity of the anticancer drug elesclomol is due to oxidative stress indirectly mediated through its complex with Cu (II). J Inorg Biochem 2014; 137: 22-30.
[25] Du Z and Lovly CM. Mechanisms of receptor tyrosine kinase activation in cancer. Mol Cancer 2018; 17: 58.
[26] De Craene B and Berx G. Regulatory networks defining EMT during cancer initiation and progression. Nat Rev Cancer 2013; 13: 97-110.
[27] Nakayama KI and Nakayama K. Ubiquitin ligases: cell-cycle control and cancer. Nat Rev Cancer 2006; 6: 369-81.
[28] Che X, Qi X, Xu Y, Wang Q and Wu G. Genomic and transcriptome analysis to identify the role of the mtor pathway in kidney renal clear cell carcinoma and its potential therapeutic significance. Oxid Med Cell Longev 2021; 2021: 6613151.
[29] Qi X, Li Q, Che X, Wang Q and Wu G. The uniqueness of clear cell renal cell carcinoma: summary of the process and abnormality of glucose metabolism and lipid metabolism in ccRCC. Front Oncol 2021; 11: 727778.
[30] Cairns P. Renal cell carcinoma. Cancer Biomark 2010; 9: 461-73.
[31] Atkins MB, Plimack ER, Puzanov I, Fishman MN, McDermott DF, Cho DC, Vaishampayan U, George S, Olencki TE, Tarazi JC, Rosbrook B, Fernandez KC, Lechuga M and Choueiri TK. Axitinib in combination with pembrolizumab in patients with advanced renal cell cancer: a non-randomised, open-label, dose-finding, and dose-expansion phase 1b trial. Lancet Oncol 2018; 19: 405-415.
[32] Wang Q, Wu G, Che X, Li Q, Zhang Z and Tang Q. Sorafenib induces renal cell carcinoma apoptosis via upregulating activating transcription factor 4. Pharmazie 2018; 73: 156-160.
[33] Mallik R and Chowdhury TA. Metformin in cancer. Diabetes Res Clin Pract 2018; 143: 409-419.
[34] Chamoto K, Al-Habsi M and Honjo T. Role of PD-1 in immunity and diseases. Curr Top Microbiol Immunol 2017; 410: 75-97.
[35] Mikami S, Mizuno R, Kondo T, Shinohara N, Nonomura N, Ozono S, Eto M, Tatsugami K, Takayama T, Matsuyama H, Kishida T and Oya M; Japanese Society of Renal Cancer. Clinical significance of programmed death-1 and programmed death-ligand 1 expression in the tumor microenvironment of clear cell renal cell carcinoma. Cancer Sci 2019; 110: 1820-1828.
[36] Yarchoan M, Hopkins A and Jaffee EM. Tumor mutational burden and response rate to PD-1 inhibition. N Engl J Med 2017; 377: 2500-2501.
[37] Miao D, Margolis CA, Gao W, Voss MH, Li W, Martini DJ, Norton C, Bossé D, Wankowicz SM, Cullen D, Horak C, Wind-Rotolo M, Tracy A, Giannakis M, Hodi FS, Drake CG, Ball MW, Allaf ME, Snyder A, Hellmann MD, Ho T, Motzer RJ, Signoretti S, Kaelin WG Jr, Choueiri TK and Van Allen EM. Genomic correlates of response to immune checkpoint therapies in clear cell re-

nal cell carcinoma. Science 2018; 359: 801-806.
[38] Braun DA, Hou Y, Bakouny Z, Ficial M, Sant' Angelo M, Forman J, Ross-Macdonald P, Berger AC, Jegede OA, Elagina L, Steinharter J, Sun M, Wind-Rotolo M, Pignon JC, Cherniack AD, Lichtenstein L, Neuberg D, Catalano P, Freeman GJ, Sharpe AH, McDermott DF, Van Allen EM, Signoretti S, Wu CJ, Shukla SA and Choueiri TK. Interplay of somatic alterations and immune infiltration modulates response to PD-1 blockade in advanced clear cell renal cell carcinoma. Nat Med 2020; 26: 909-918.
[39] Ghatalia P, Gordetsky J, Kuo F, Dulaimi E, Cai KQ, Devarajan K, Bae S, Naik G, Chan TA, Uzzo R, Hakimi AA, Sonpavde G and Plimack E. Prognostic impact of immune gene expression signature and tumor infiltrating immune cells in localized clear cell renal cell carcinoma. J Immunother Cancer 2019; 7: 139.
[40] Jonasch E, Walker CL and Rathmell WK. Clear cell renal cell carcinoma ontogeny and mechanisms of lethality. Nat Rev Nephrol 2021; 17: 245-261.
[41] Harlander S, Schönenberger D, Toussaint NC, Prummer M, Catalano A, Brandt L, Moch H, Wild PJ and Frew IJ. Combined mutation in Vhl, Trp53 and Rb1 causes clear cell renal cell carcinoma in mice. Nat Med 2017; 23: 869-877.
[42] Gossage L, Eisen T and Maher ER. VHL, the story of a tumour suppressor gene. Nat Rev Cancer 2015; 15: 55-64.
[43] Tian T, Li X and Zhang J. mTOR signaling in cancer and mTOR inhibitors in solid tumor targeting therapy. Int J Mol Sci 2019; 20: 755.
[44] Murugan AK. mTOR: role in cancer, metastasis and drug resistance. Semin Cancer Biol 2019; 59: 92-111.
[45] Bailey ST, Smith AM, Kardos J, Wobker SE, Wilson HL, Krishnan B, Saito R, Lee HJ, Zhang J, Eaton SC, Williams LA, Manocha U, Peters DJ, Pan X, Carroll TJ, Felsher DW, Walter V, Zhang Q, Parker JS, Yeh JJ, Moffitt RA, Leung JY and Kim WY. MYC activation cooperates with Vhl and Ink4a/Arf loss to induce clear cell renal cell carcinoma. Nat Commun 2017; 8: 15770.
[46] Jiang L, Kon N, Li T, Wang SJ, Su T, Hibshoosh H, Baer R and Gu W. Ferroptosis as a p53-mediated activity during tumour suppression. Nature 2015; 520: 57-62.
[47] Yu S, Dai J, Ma M, Xu T, Kong Y, Cui C, Chi Z, Si L, Tang H, Yang L, Sheng X and Guo J. RBCK1 promotes p53 degradation via ubiquitination in renal cell carcinoma. Cell Death Dis 2019; 10: 254.
[48] Zhang C, Liu J, Liang Y, Wu R, Zhao Y, Hong X, Lin M, Yu H, Liu L, Levine AJ, Hu W and Feng Z. Tumour-associated mutant p53 drives the Warburg effect. Nat Commun 2013; 4: 2935.
[49] Zhao C, Dong H, Xu Q and Zhang Y. Histone deacetylase (HDAC) inhibitors in cancer: a patent review (2017-present). Expert Opin Ther Pat 2020; 30: 263-274.
[50] Alves-Fernandes DK and Jasiulionis MG. The role of SIRT1 on DNA damage response and epigenetic alterations in cancer. Int J Mol Sci 2019; 20: 3153.
[51] Chang HC and Guarente L. SIRT1 and other sirtuins in metabolism. Trends Endocrinol Metab 2014; 25: 138-45.
[52] Prozorovski T, Schulze-Topphoff U, Glumm R, Baumgart J, Schröter F, Ninnemann O, Siegert E, Bendix I, Brüstle O, Nitsch R, Zipp F and Aktas O. Sirt1 contributes critically to the redox-dependent fate of neural progenitors. Nat Cell Biol 2008; 10: 385-94.
[53] Le DT, Durham JN, Smith KN, Wang H, Bartlett BR, Aulakh LK, Lu S, Kemberling H, Wilt C, Luber BS, Wong F, Azad NS, Rucki AA, Laheru D, Donehower R, Zaheer A, Fisher GA, Crocenzi TS, Lee JJ, Greten TF, Duffy AG, Ciombor KK, Eyring AD, Lam BH, Joe A, Kang SP, Holdhoff M, Danilova L, Cope L, Meyer C, Zhou S, Goldberg RM, Armstrong DK, Bever KM, Fader AN, Taube J, Housseau F, Spetzler D, Xiao N, Pardoll DM, Papadopoulos N, Kinzler KW, Eshleman JR, Vogelstein B, Anders RA and Diaz LA Jr. Mismatch repair deficiency predicts response of solid tumors to PD-1 blockade. Science 2017; 357: 409-413.
[54] Asaoka Y, Ijichi H and Koike K. PD-1 blockade in tumors with mismatch-repair deficiency. N Engl J Med 2015; 373: 1979.
[55] Liu W, Ren D, Xiong W, Jin X and Zhu L. A novel FBW7/NFAT1 axis regulates cancer immunity in sunitinib-resistant renal cancer by inducing PD-L1 expression. J Exp Clin Cancer Res 2022; 41: 38.
[56] Zhu G, Pei L, Li Y and Gou X. EP300 mutation is associated with tumor mutation burden and promotes antitumor immunity in bladder cancer patients. Aging (Albany NY) 2020; 12: 2132-2141.
[57] Wang X, Duanmu J, Fu X, Li T and Jiang Q. Analyzing and validating the prognostic value and mechanism of colon cancer immune microenvironment. J Transl Med 2020; 18: 324.
[58] Ribas A and Wolchok JD. Cancer immunotherapy using checkpoint blockade. Science 2018; 359: 1350-1355.
[59] Tang D, Kang R, Berghe TV, Vandenabeele P and Kroemer G. The molecular machinery of regulated cell death. Cell Res 2019; 29: 347-364.
[60] D'Arcy MS. Cell death: a review of the major forms of apoptosis, necrosis and autophagy. Cell Biol Int 2019; 43: 582-592.

[61] Chen X, Li J, Kang R, Klionsky DJ and Tang D. Ferroptosis: machinery and regulation. Autophagy 2021; 17: 2054-2081.
[62] Kovacs SB and Miao EA. Gasdermins: effectors of pyroptosis. Trends Cell Biol 2017; 27: 673-684.
[63] Kahlson MA and Dixon SJ. Copper-induced cell death. Science 2022; 375: 1231-1232.
[64] Kim JH, Alderson TR, Frederick RO and Markley JL. Nucleotide-dependent interactions within a specialized Hsp70/Hsp40 complex involved in Fe-S cluster biogenesis. J Am Chem Soc 2014; 136: 11586-9.
[65] Sheftel AD, Stehling O, Pierik AJ, Elsässer HP, Mühlenhoff U, Webert H, Hobler A, Hannemann F, Bernhardt R and Lill R. Humans possess two mitochondrial ferredoxins, Fdx1 and Fdx2, with distinct roles in steroidogenesis, heme, and Fe/S cluster biosynthesis. Proc Natl Acad Sci U S A 2010; 107: 11775-80.
[66] Wu G, Wang Q, Xu Y, Li Q and Cheng L. A new survival model based on ferroptosis-related genes for prognostic prediction in clear cell renal cell carcinoma. Aging (Albany NY) 2020; 12: 14933-14948.
[67] Qi X, Lv X, Wang X, Ruan Z, Zhang P, Wang Q, Xu YM and Wu G. A new survival model based on cholesterol biosynthesis-related genes for prognostic prediction in clear cell renal cell carcinoma. Biomed Res Int 2021; 2021: 9972968.
[68] Wettersten HI, Aboud OA, Lara PN Jr and Weiss RH. Metabolic reprogramming in clear cell renal cell carcinoma. Nat Rev Nephrol 2017; 13: 410-419.
[69] Zheng L, Han P, Liu J, Li R, Yin W, Wang T, Zhang W and Kang YJ. Role of copper in regression of cardiac hypertrophy. Pharmacol Ther 2015; 148: 66-84.
[70] Mandinov L, Mandinova A, Kyurkchiev S, Kyurkchiev D, Kehayov I, Kolev V, Soldi R, Bagala C, de Muinck ED, Lindner V, Post MJ, Simons M, Bellum S, Prudovsky I and Maciag T. Copper chelation represses the vascular response to injury. Proc Natl Acad Sci U S A 2003; 100: 6700-5.
[71] Hoefflin R, Harlander S, Schäfer S, Metzger P, Kuo F, Schönenberger D, Adlesic M, Peighambari A, Seidel P, Chen CY, Consenza-Contreras M, Jud A, Lahrmann B, Grabe N, Heide D, Uhl FM, Chan TA, Duyster J, Zeiser R, Schell C, Heikenwalder M, Schilling O, Hakimi AA, Boerries M and Frew IJ. HIF-1α and HIF-2α differently regulate tumour development and inflammation of clear cell renal cell carcinoma in mice. Nat Commun 2020; 11: 4111.
[72] Yang F, Zhang H, Mei Y and Wu M. Reciprocal regulation of HIF-1α and lincRNA-p21 modulates the Warburg effect. Mol Cell 2014; 53: 88-100.
[73] Barata PC and Rini BI. Treatment of renal cell carcinoma: current status and future directions. CA Cancer J Clin 2017; 67: 507-524.
[74] Yang Z, Yang X, Xu S, Jin P, Li X, Wei X, Liu D, Huang K, Long S, Wang Y, Sun C, Chen G, Hu J, Meng L, Ma D and Gao Q. Reprogramming of stromal fibroblasts by SNAI2 contributes to tumor desmoplasia and ovarian cancer progression. Mol Cancer 2017; 16: 163.
[75] Lee JH, Liu R, Li J, Wang Y, Tan L, Li XJ, Qian X, Zhang C, Xia Y, Xu D, Guo W, Ding Z, Du L, Zheng Y, Chen Q, Lorenzi PL, Mills GB, Jiang T and Lu Z. EGFR-phosphorylated platelet isoform of phosphofructokinase 1 promotes PI3K activation. Mol Cell 2018; 70: 197-210, e7.
[76] Tavera-Montañez C, Hainer SJ, Cangussu D, Gordon SJV, Xiao Y, Reyes-Gutierrez P, Imbalzano AN, Navea JG, Fazzio TG and Padilla-Benavides T. The classic metal-sensing transcription factor MTF1 promotes myogenesis in response to copper. FASEB J 2019; 33: 14556-14574.
[77] Chen PH, Wu J, Ding CC, Lin CC, Pan S, Bossa N, Xu Y, Yang WH, Mathey-Prevot B and Chi JT. Kinome screen of ferroptosis reveals a novel role of ATM in regulating iron metabolism. Cell Death Differ 2020; 27: 1008-1022.
[78] Bhalla S, Chaudhary K, Kumar R, Sehgal M, Kaur H, Sharma S and Raghava GP. Gene expression-based biomarkers for discriminating early and late stage of clear cell renal cancer. Sci Rep 2017; 7: 44997.
[79] Xv Y, Lv F, Guo H, Liu Z, Luo D, Liu J, Gou X, He W, He W and Zheng Y. A CT-based radiomics nomogram integrated with clinic-radiological features for preoperatively predicting WHO/ISUP grade of clear cell renal cell carcinoma. Front Oncol 2021; 11: 712554.
[80] Yi X, Xiao Q, Zeng F, Yin H, Li Z, Qian C, Wang C, Lei G, Xu Q, Li C, Li M, Gong G, Zee C, Guan X, Liu L and Chen BT. Computed tomography radiomics for predicting pathological grade of renal cell carcinoma. Front Oncol 2021; 10: 570396.
[81] Researchers strive to refine TMB. Cancer Discov 2021; 11: 1314.
[82] Valero C, Lee M, Hoen D, Wang J, Nadeem Z, Patel N, Postow MA, Shoushtari AN, Plitas G, Balachandran VP, Smith JJ, Crago AM, Long Roche KC, Kelly DW, Samstein RM, Rana S, Ganly I, Wong RJ, Hakimi AA, Berger MF, Zehir A, Solit DB, Ladanyi M, Riaz N, Chan TA, Seshan VE and Morris LGT. The association between tumor mutational burden and prognosis is dependent on treatment context. Nat Genet 2021; 53: 11-15.